Transmission-Line Model of Non-Uniform Leaky-Wave Antennas

Nghia Nguyen-Trong, *Student Member, IEEE,* Leonard Hall, *Member, IEEE,* and Christophe Fumeaux, *Senior Member, IEEE*

***Abstract*—Non-uniform leaky-wave antennas (LWAs) are analyzed and synthesized using a lossy transmission line model. The analysis is based on a general waveguide circuit theory. Compared to the classical approach, the model yields a higher accuracy in the computation of both aperture field distribution and radiation patterns. The proposed analysis is also able to provide scattering parameters of the whole structure in a fraction of a second, which is valuable for antenna optimization. Based on the analysis, a general method for far-field pattern synthesis utilizing global optimization is presented. As an application demonstration, the Half-Mode Substrate-Integrated Waveguide, or half-width microstrip line, has been selected as basis structure for the LWA designs. Two antennas have been optimized targeting different specifications, i.e. a low sidelobe level and a wide null in the radiation pattern. Experimental results are provided for these selected examples of non-uniform LWAs, which ultimately validate the proposed technique as an improvement over the classical approach.**

***Index Terms*—Leaky-wave antenna (LWA), pattern synthesis, transmission line model, non-uniform structure, Half-Mode Substrate-Integrated Waveguide (HMSIW), half-width microstrip line.**

I. Introduction

THE general analysis method for leaky-wave antennas (LWAs) was first introduced in [1] and has been covered in many antenna textbooks such as [2], [3]. This analysis method has been used widely in the literature for design and pattern synthesis due to its simplicity and reasonable prediction on the antenna radiation patterns such as in [4]–[6]. Nevertheless, the analysis relies on simplifying assumptions, which have to be emphasized and recognized, otherwise inaccurate prediction on both near-field and far-field distributions could be obtained (these assumptions will be discussed in the next section). To achieve a more accurate analysis, a different technique to analyze non-uniform LWAs with smooth profile variations is proposed based on a general waveguide circuit theory propounded by Marks and Williams in 1992 [7].

The method proposed in this paper is a generalization of [8], in which the authors analyzed and optimized a specific leaky-wave structure targeting wideband operation. The main contribution of [8] is the optimization of reflection coefficient of the Half-Mode Substrate-Integrated Waveguide (HMSIW) over a wide range of frequency. It is noted that the analysis in [8] implicitly employed the concept of power-wave [9] and its parameter conversion table [10]. Despite providing reasonably accurate results in most cases, this is indeed not the best theory to handle traveling-wave due to the discontinuity property of the power-wave [7], [11], [12]. To avoid the use of power wave and bypass this issue, the present paper provides a thorough analysis of a LWA based on a general waveguide circuit theory of traveling-wave as found in [7]. The assumption of this analysis is that only a single mode is propagating along the waveguide.

Based on the proposed analysis, far-field pattern synthesis utilizing global optimization is demonstrated. The method shows higher flexibility in the design process compared to the classical LWA analysis approach [1]–[3]. Utilizing this method, a pattern synthesis can be carried out without the necessity of independent control on attenuation constant $\alpha(z)$ and phase constant $\beta(z)$ along the antenna length, such as in [6], [13]. For illustration, two LWAs have been optimized targeting two different specifications, namely a low sidelobe level and a wide null in far-field pattern, applying the method on a simple leaky-structure, i.e. the HMSIW. For validation, these two antennas have been fabricated and their performance is compared with analytical results demonstrating high degree of agreement. Our recent conference paper [14] presented a preliminary study on the optimization for low sidelobe level LWA verified by full-wave simulation. As a significant extension to [14], this paper provides the complete theory, further optimizations and thorough experimental validation.

The paper will start by revising the classical approach on analyzing a general LWA, through which the assumptions on the model will be discussed. Then the proposed analysis will be presented in section III with a brief validation on the near-field distribution and a process to incorporate a feeding transition into the analysis. Section IV will illustrate the general procedure of pattern synthesis utilizing global optimization. Using this process, section V will present two specific designs followed by experimental validation and further discussion.

II. Classical Analysis of LWA

Although the classical analysis of LWAs is well-known, its main aspects will be briefly revised in this section to emphasize the critical assumptions employed in the analysis.

A continuous-source LWA is described by the varying propagation constant $\gamma(z) = \alpha(z) + j\beta(z)$ along the guiding direction, i.e. z-direction. Here $\gamma(z)$ can be calculated using

N. Nguyen-Trong and C. Fumeaux are with School of Electrical and Electronic Engineering, University of Adelaide, Australia, 5005 email: nghia.nguyentrong@adelaide.edu.au.

L. Hall is with Defence Science and Technology Organisation (DSTO), Australia, 5111.

C. Fumeaux acknowledges the support of the Australian Research Council (ARC) Future Fellowship funding scheme (under FT100100585).

various analysis methods such as transverse resonance method (TRM), variational method (VM) [2] or modal analysis [15]. Alternatively, it can also be obtained through simulation [16]–[19] or experiment [2].

For the analysis of the radiation properties of a LWA, the source distribution function $A(z) = |A(z)|e^{j\psi(z)}$ is required to be computed. Here $A(z)$ is the equivalent current traveling along the antenna with phase $\psi(z)$. The radiation pattern can be readily calculated as a Fourier transform of $A(z)$ [2]. Thus, in this analysis, $A(z)$ is directly linked to the near-field distribution of the LWA.

The aim is to determine $A(z)$ from $\gamma(z)$. The traditional approach relates the attenuation constant α with the power along the source

$$2\alpha(z) = -\frac{1}{P(z)}\frac{dP(z)}{dz}. \tag{1}$$

For simplicity, assuming the lossless case (only radiation loss is present), $p_R = -dP(z)/dz$ can be interpreted as the power radiated per unit length. Therefore, p_R may be written as

$$p_R = C|A(z)|^2. \tag{2}$$

Combining these two equations, one can easily arrive at

$$|A(z)|^2 = \frac{1}{C}\alpha(z)e^{-2\int_0^z \alpha(\tau)d\tau}. \tag{3}$$

The phase $\psi(z)$ is simply

$$\psi(z) = -\int_0^z \beta(\tau)d\tau. \tag{4}$$

As Walter pointed out in Chapter 4 of [2], equation (2) is only true when considering the infinitesimal element dz radiating in isolation. This means the above analysis neglects the reflections along a non-uniform structure and is only an approximation for traveling-waves [2]. Furthermore, the constant of proportionality C for an infinitesimal element dz is also assumed to be constant along the antenna, which is apparently not correct if the cross-section varies.

In summary, although the classical analysis is simple and provides a closed-form solution for the source distribution of any LWA, the aforementioned assumptions should always be considered before application. Under these assumptions, the classical analysis does not determine the true field propagating along the LWA. Instead, it links radiated power intensity to the magnitude of source distribution, i.e. equation (2). One of the biggest advantages of this analysis is that only the propagation constant $\gamma(z)$ is required to be computed. Modal field analysis is only needed to some extent in order to identify the polarization of the LWA radiation pattern.

III. Transmission-Line Model of LWA

In this section, the analysis of a LWA based on the circuit waveguide theory found in [7] will be described first, followed by a brief validation on the near-field distribution of a chosen continuous-source leaky-wave structure, i.e. the HMSIW. The last subsection will illustrate a process to include a transition structure for accuracy improvement.

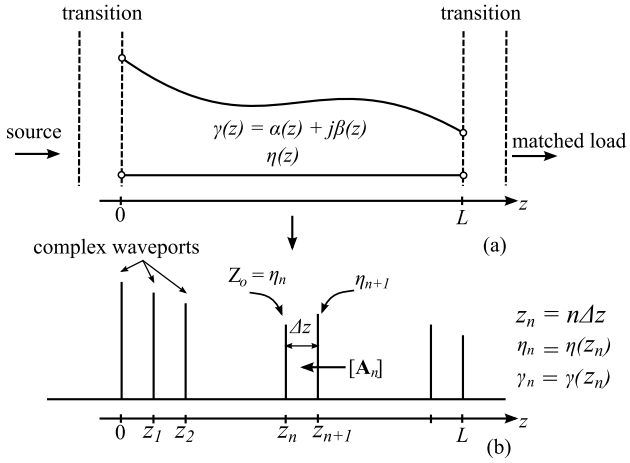

Fig. 1. (a) A generic representation of non-uniform LWA: $\gamma(z)$ is the propagation constant along the antenna, η is the wave impedance which can be calculated from γ depending on the propagating mode, L is the antenna length; (b) Discretized model to analyze a non-uniform LWA.

A. Model and Analysis

The present analysis treats the smoothly varying non-uniform LWA as a lossy transmission line (TL) with variable complex impedance and propagation constant along its length. Therefore, the theoretical framework described in [7], which provides an accurate circuit model for traveling-wave structures is applied. Since a circuit model with voltage and current waves is involved, the analysis assumes a single mode propagating along the wave-guiding structure. This is a reasonable assumption since for many LWAs designed in the single-mode operation region of their host waveguide (so that only one set of propagation constant $\gamma(z)$ is considered). A generic non-uniform continuous-source LWA is illustrated in Fig. 1a.

The general idea of the analysis is to discretize the LWA into small sections which can be then approximated as uniform transmission lines (UTL). These small sections (illustrated Fig. 1b) can then be cascaded to obtain the network parameters of the whole structure. This would have been straightforward if the characteristic impedances would be real, but this is not the case for LWAs - hence the theory in [7] is utilized. It is emphasized that although the general concept is based on [8], the present analysis shows a much more systematic approach and is general for a traveling-wave in a lossy single-mode transmission line. For completeness, we summarize the circuit model for a uniform lossy waveguide first and then demonstrate how it can be applied to calculate the field distribution along a non-uniform LWA.

1) Circuit model for a uniform section: In contrast to the traditional approach, this model actually examines the physical field of a traveling-wave [7]

$$\mathbf{E}_t = c_+e^{-\gamma z}\mathbf{e}_t + c_-e^{\gamma z}\mathbf{e}_t \equiv \frac{v(z)}{v_0}\mathbf{e}_t \tag{5}$$

$$\mathbf{H}_t = c_+e^{-\gamma z}\mathbf{h}_t - c_-e^{\gamma z}\mathbf{h}_t \equiv \frac{i(z)}{i_0}\mathbf{h}_t \tag{6}$$

where $\mathbf{e}_t$ and $\mathbf{h}_t$ are the normalized transverse modal field distribution, which are independent on z in a uniform section;

v_0 and i_0 are normalization constant of the waveguide voltage $v(z)$ and current $i(z)$. The normalization constant for power and characteristic impedance are respectively [7]

$$p_0 = \int_S \mathbf{e}_t \times \mathbf{h}_t^* \cdot \hat{\mathbf{z}} dS = v_0 i_0^* \tag{7}$$

$$Z_0 = v_0/i_0 = |v_0|^2/p_0^* = p_0/|i_0|^2 = \frac{|v_0|^2}{\int_S |\mathbf{e}_t|^2 dS}\eta. \tag{8}$$

where η is the wave impedance, which satisfies $\hat{\mathbf{z}} \times \mathbf{e}_t = \eta \mathbf{h}_t$ and S is the cross-section of the waveguide, which in an assumption is the whole transverse plane for a LWA. When formulating this circuit model for a UTL, v_0 can be chosen arbitrarily and the modal field $\mathbf{e}_t$ can be normalized by any non-zero constant. Thus, only the phase of Z_0 is fixed, which is the same as that of the wave impedance η. The forward and backward traveling wave intensities are then defined respectively as

$$a_0 \equiv \frac{\sqrt{Re(p_0)}}{2v_0}(v + iZ_0);\ b_0 \equiv \frac{\sqrt{Re(p_0)}}{2v_0}(v - iZ_0) \tag{9}$$

By this definition, the traveling-wave is continuous and thus, it is possible to cascade series-connected two-port networks.

2) Field distribution calculation: The LWA is discretized into small sections as illustrated in Fig. 1b. Each interface between two adjacent sections is treated as one waveguide port. At each port, v_0 and $\mathbf{e}_t$ can always be selected and normalized such that

$$v_0(z) = 1 \text{ and } \int_S |\mathbf{e}_t(z)|^2 dS = 1. \tag{10}$$

This simple choice makes the characteristic impedance identical to the wave impedance $Z_0 = \eta$ (see equation (8)). The normalized constant of the traveling-wave intensity in equation (9) is then reduced to

$$\frac{\sqrt{Re(p_0(z))}}{2v_0(z)} = \frac{\sqrt{Re(\eta(z))}}{2|\eta(z)|}. \tag{11}$$

This is very convenient since $\eta(z)$ can be calculated from $\gamma(z)$ depending on the propagating mode of the traveling-wave.

At this stage, all necessary normalization parameters are defined, and the analysis can proceed as follows: The ABCD-matrix of each approximately uniform section is calculated as

$$\begin{aligned}[\mathbf{A_n}] &= \begin{bmatrix} A_n & B_n \\ C_n & D_n \end{bmatrix} \\ &\approx \begin{bmatrix} \cosh(\gamma_n \Delta z) & \eta_n \sinh(\gamma_n \Delta z) \\ \frac{1}{\eta_n}\sinh(\gamma_n \Delta z) & \cosh(\gamma_n \Delta z) \end{bmatrix}. \end{aligned} \tag{12}$$

Fig. 1b defines and illustrates how $[\mathbf{A_n}]$ is computed from γ_n and η_n.

The voltage at a particular position z_x along the antenna is calculated from the S-parameters of two series-connected two-port networks as illustrated in Fig. 2. These S-parameters are obtained by converting the corresponding cascaded ABCD-matrices with two complex port impedances [7] (see Appendix). Under the normalization of (10), the two equations in (9) can be combined to yield

$$v(z_x) = \frac{|\eta_x|}{\sqrt{Re(\eta_x)}}(a_x + b_x), \tag{13}$$

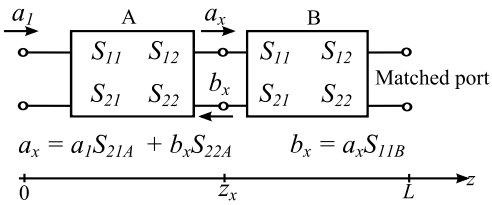

Fig. 2. Two series-connected two port network for the calculation of the voltage at the junction

where η_x is the wave impedance at $z = z_x$. By relating a_x with a_1 and b_x using S-parameters of each section A and B, $v(z_x)$ can be obtained from (Fig. 2)

$$a_x + b_x = (S_{11B} + 1)\frac{S_{21A}}{1 - S_{22A}S_{11B}} a_1. \tag{14}$$

Let $v(0)^+$ and $\eta(0)$ be the forward voltage and the wave impedance at $z = 0$. From (13) and (14), the voltage at any position along the antenna is

$$v(z_x) = v(0)^+ (S_{11B} + 1)\frac{S_{21A}}{1 - S_{22A}S_{11B}} \frac{|\eta_x|}{|\eta(0)|}\sqrt{\frac{Re(\eta(0))}{Re(\eta_x)}}. \tag{15}$$

It is noted that the calculation of these S-parameters can be carried out simultaneously when cascading the ABCD-parameters of each section.

From equation (5), $\mathbf{E}_t$ can be obtained as

$$\mathbf{E}_t(z) = \frac{v(z)}{v_0}\mathbf{e}_t = v(z)\mathbf{e}_t(z). \tag{16}$$

Hence, the electric field $\mathbf{E}_t$ can be calculated if $\mathbf{e}_t$ is known, provided $\int_S |\mathbf{e}_t(z)|^2 dS = 1$. Typically, finding $\mathbf{e}_t$ requires solving a boundary condition problem in 2 dimensions. For typical LWAs, a reasonable approximation can be made considering that a leaky-wave structure is a perturbation from a waveguide for which an exact solution of modal field is available. Thus, a good estimation is $\mathbf{e}_t \approx \mathbf{e}_{0t}$ where $\mathbf{e}_{0t}$ is the unperturbed modal solution. Furthermore, provided that the cross-section does not vary significantly along the LWA, one may just approximate $\mathbf{e}_t$ as constant versus position, in which case the field becomes simply proportional to the voltage $v(z)$.

B. Near-field Validation

As an initial validation, the near-field distribution will be calculated using the proposed method in comparison with the traditional approach and simulations using full-wave numerical software Ansys HFSS. The first structure chosen for investigation is the HMSIW [18], which can be alternatively classified as a half-width microstrip line [20] (Fig. 3a). This waveguide has been utilized extensively to design LWAs such as in [21]–[27]. The particular example is chosen here due to its simplicity, ease of fabrication and continuous-source profile. An accurate solution for propagation constant of an ideal HMSIW, i.e. with infinite ground plane and semi-infinite top conductive layer is available [28], [29]. The fundamental mode of a HMSIW is the half-mode $TE_{0,0.5}$, thus the wave impedance is calculated as

$$\eta_{TE}(z) = \frac{j}{\omega\gamma(z)}. \tag{17}$$

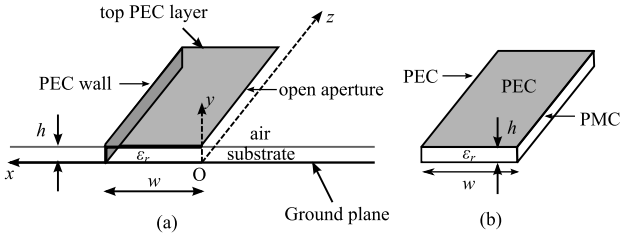

Fig. 3. The HMSIW (a) and its corresponding unperturbed structure (b). The PEC wall can be realized by via-holes with accurate width conversion formula [30].

For demonstration of improvement over the classical analysis, a HMSIW with non-uniform profile is considered. The selected material is Rogers Duroid 5880 with relative permittivity $\epsilon_r = 2.2$ and thickness $h = 31$ mil $= 0.787$ mm. The antenna length is chosen as $L = 200$ mm. A simple linear width profile is selected as

$$w(z) \quad = \quad w_{start}(1 - Kz) \tag{18}$$

where the tapering constant $K = (w_{start} - w_{end})/L$ and w_{start} and w_{end} are start and end widths of the HMSIW. The voltage $v(z)$ along the waveguide is then obtained following the analysis of the previous subsection III-A. To determine the waveguide field distribution, the HMSIW can be considered as a perturbation from an ideal rectangular waveguide with a perfect magnetic conductor at one side as illustrated in Fig. 3b. Therefore, the modal electric field $\mathbf{e}_t$ can be written approximately as

$$\mathbf{e}_t(x, y, z) \approx \sqrt{\frac{1}{w(z)h}} \cos(\frac{\pi x}{2w(z)}) \cdot \hat{\mathbf{y}}, \tag{19}$$

in which the normalization condition in equation (10) is also satisfied. Thus, the field distribution at the antenna aperture $(x = 0)$ can be approximated as

$$\mathbf{E}(x = 0) \propto \frac{v(z)}{\sqrt{w(z)}}\hat{\mathbf{y}}. \tag{20}$$

Fig. 4 shows the analysis and simulation for the aperture field distribution at $f = 8$ GHz for $w_{start} = 9$ mm, $L = 200$ mm and $w_{end} = 5$ mm ($K = 0.02$). Excellent agreement can be observed between the proposed analysis and the corresponding simulation, which validates the accuracy and correctness of the analysis. From the results, three expected physical features can be noticed:

1) The distributed reflections along the waveguide due to the tapering effect result in a standing-wave.
2) The structure radiates extensively when the length reaches a certain value, i.e. $z \geq 160$ mm. This is because α starts increasing sharply as the width is reduced close to the cut-off of the waveguide [18].
3) Before this position of extensive radiation, the field strength increases slightly along z since the width is decreased and the power density should be increased (without much radiation).

The results for the source of radiations using traditional approach (Section II) is also included in Fig. 4. It can be

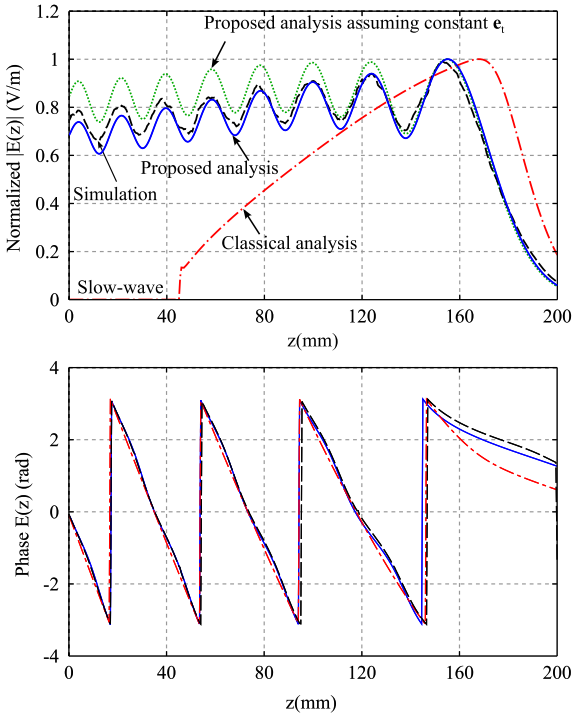

Fig. 4. Normalized aperture field ($x = 0$) of the a tapered HMSIW at $f = 8$ GHz for $w_{start} = 9$ mm, $L = 200$ mm and $w_{end} = 5$ mm ($K = 0.02$): (a) Magnitude; (b) Phase. The legend is the same for both figures: solid lines for proposed analysis; dotted lines for proposed analysis assuming constant $\mathbf{e}_t$; dot-dashed line for classical analysis and dashed lines for simulation.

observed that the classical analysis result exhibits a large discrepancy compared to simulation. This is as expected from the assumptions that are applied in (2). In Fig. 4, when $z \in (0, 45)$ mm, the classical analysis yields zero field distribution because $\alpha(z) = 0$ in this region, i.e. the slow-wave region (see (3)). These considerations take into account the fact that the slow-wave does not radiate and this part can thus be excluded in the calculation of the near-field and far-field. This is however not rigorously true because the non-radiating property of slow-wave is only exact for infinitely long and continuous waveguide. As soon as non-uniformity or discontinuities are included, which is the case for any finite-length LWA, radiation (even if weak) will occur.

It can be noticed further that if the cross-section along the antenna does not vary significantly, it is possible to simply approximate $\mathbf{E} \propto v(z)\hat{\mathbf{u}}$ where $\hat{\mathbf{u}}$ is the unit vector of electric field polarization. As demonstrated in Fig. 4a (dotted line), this still provides a reasonable approximation on the aperture field distribution of the antenna. More validation on the near-field will be shown in a later section (Section V-A). We also note that the near-field distribution of this type of tapered LWA has been validated through experiment in [31].

Using the field equivalence principle, the source distribution of a LWA, i.e. the equivalent current, can be shown to be proportional to near-field distribution. In summary, based only on the knowledge of the propagation constant $\gamma(z)$ (just as similar to the classical approach), using the proposed analysis, one can always obtain a much more accurate prediction on

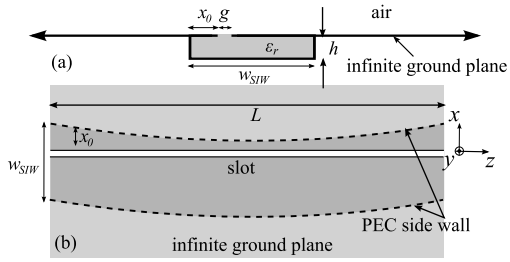

Fig. 5. A slotted SIW LWA with meadering side walls [32]: (a) Cross-section; (b) Top view.

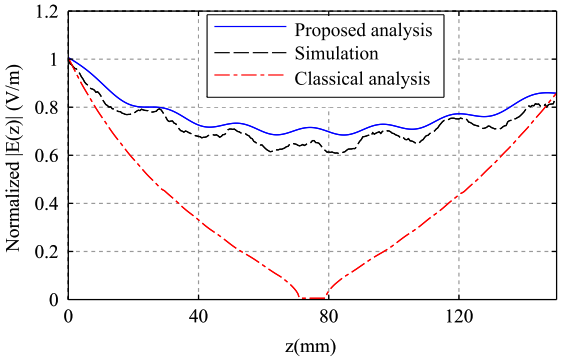

Fig. 6. Normalized magnitude of aperture electric field ($x = 0$) of a non-uniform slotted SIW.

the radiation source distribution of a LWA than the traditional approach (using $\mathbf{E} \propto v(z)\hat{\mathbf{u}}$). A very accurate prediction of the field can be obtained if a close approximation of the modal field is available, e.g. as provided in this case through (19).

As a validation for the generality of the method, a different LWA based on a meandering substrate-integrated waveguide (SIW) with continuous longitudinal slot [32] is also investigated in this section. As proposed in [32], to reduce the cross-polarization, the slot is kept straight while the shape of the PEC side walls is altered along the waveguide (Fig 5). The width of SIW is kept constant as $w_{SIW} = 10$ mm. Other parameters are substrate thickness $h = 0.787$ mm, relative permittivity $\epsilon_r = 2.2$, antenna length $L = 150$ mm and slot width $g = 0.2$ mm. The shape of the SIW is defined using parameter x_0, which is chosen in this investigation case as a cosine function

$$x_0(z) = k_1 + k_2 \sin(\frac{\pi z}{L}). \tag{21}$$

The propagation constant of this structure is calculated approximately using the variational method proposed in [33]. Fig. 6 shows the analyzed and simulated electric field distribution on the slot at $f = 7$ GHz for the case $k_1 = 2.5$ mm and $k_2 = -2$ mm. Similar features as for the previous case (the HMSIW) can be observed, which further demonstrates the general applicability of the proposed model.

C. Method Limitation for Rapidly Changing Structure

As stated in Section III-A, the assumption for the proposed analysis is that only one mode is propagating along the waveguide. This implies that the results will degrade for increasingly rapid profile variations of the leaky-wave structure,

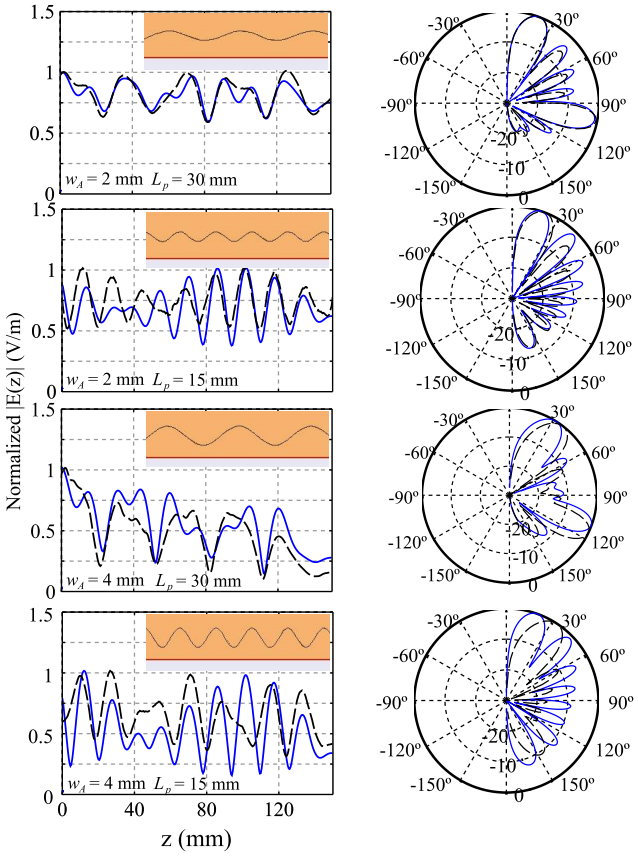

Fig. 7. Normalized magnitude of aperture field of more rapidly changing HMSIWs and the corresponding normalized radiation pattern at $f = 8$ GHz (width profile shown in equation (22), $w_0 = 9$ mm, $L = 150$ mm). Blue solid lines: analysis, black dashed lines: simulation. The insets show top views with the same scale of the width and length of the HMSIWs.

as these can excite higher-order modes. In order to illustrate this feature, a HMSIW with the width profile

$$w(z) = w_0 - w_A \sin(\frac{2\pi z}{L_p}) \tag{22}$$

is considered. The highest variation in the width is $w_{\max}/w_{\min} = (w_0 + w_A)/(w_0 - w_A)$ and the maximum slope of the width with respect to the guiding direction is $2\pi w_A/L_p$. Figure 7 shows the analyzed and simulated near-field distribution at $f = 8$ GHz (wavelength $\lambda = 37.5$ mm) for different values of w_A and L_p while w_0 is fixed at 9 mm for an antenna length $L = 150$ mm. It can be confirmed from Fig. 7 that the accuracy of the analysis decreases with increasing w_A and decreasing L_p. It is noted that rapidly changing LWAs are often used in periodic structures [34], [35], which is not the general type of problem addressed in this paper. In contrast, for many of applications of continuous-source LWA structures, the method still shows an excellent agreement and high degree of improvement compared to the classical formula as further shown in later sections.

D. Inclusion of Feeding or Load Transition Structure

Typically, the feeding and load transitions can be designed to provide nearly perfect impedance matching for relative narrow band antenna. However, for wideband designs, e.g.

devices with about 80% relative bandwidth such as in [21], [24], the effect of the feeding/load transitions should be included for more accurate prediction on S-parameters. This section will demonstrate how this can be carried out with the aid of a numerical simulation tool.

The general concept is simply to obtain the ABCD-matrix of the feeding structure from simulation and then cascade it with the ABCD-matrix of the LWA (Fig. 1)

$$[\mathbf{A}_{\text{structure}}] = [\mathbf{A}_{\text{transition1}}] \cdot [\mathbf{A}_{\text{antenna}}] \cdot [\mathbf{A}_{\text{transition2}}]. \qquad (23)$$

However, extreme care needs to be taken when simulating the feed to obtain $[\mathbf{A}_{\text{transition}}]$. This is because by definition, ABCD-matrix relates the voltage and current at two ports, which in turn depend on the simulated port impedance. Furthermore, the port impedance Z_0 depends on the definition used in the simulator.

In [7], Marks and Williams showed that the scattering parameter of a traveling-wave is constant with the normalization factor of v_0. Therefore, to obtain the correct ABCD-matrix to be used in equation (23), one should simulate the transition structure using a matched port, e.g. without normalization on impedance when using ANSYS HFSS. This will yield the true S-parameter of the traveling wave. Then these obtained S-parameters can be converted into ABCD-matrix as shown in the Appendix [7]. When performing this conversion, the port impedances at the interfaces between the antenna and the transitions (Fig. 1a) are the characteristic impedances that are chosen for the LWA, i.e. $\eta(0)$ and $\eta(L)$ (Fig. 1b).

The effect of including the feeding structure will be demonstrated in Section V. It is worth emphasizing that the transition is normally designed and simulated separately from the antenna. The ABCD-matrix can be extracted once only to be placed in the pattern synthesis or any optimization process. Therefore, the above procedure can improve the accuracy for the prediction of the S-parameters of the whole structure (Section V) without noticeably increasing the design time.

IV. Far-Field Pattern Synthesis

A LWA can be considered as an array of discrete sources with infinitesimal separations [2], [36]. The far-field pattern $E(\theta)$ is calculated from the complex source distribution $A(z)$ as

$$E(\theta) = G(\theta) \int_0^L |A(z')| e^{j[\psi(z') + k_0 z' \cos\theta]} dz'. \qquad (24)$$

where $G(\theta)$ is the element pattern.

The traditional pattern synthesis is based on the fact that the far-field pattern is a Fourier transform of a near-field or source complex distribution $A(z)$ [2]. The general approach is illustrated in Fig. 8 (dotted line). However, as demonstrated in the previous sections, for non-uniform LWA, the classical analysis only yields a rough approximation of the source distribution. Furthermore, assuming that a far-field pattern $E(\theta)$ is specified, the method should also involve an iterative process since the inverse Fourier transform of $E(\theta)$ yields a field distribution $A(z)$ which is generally non-zero everywhere while the LWA always has a finite length. Finally, although closed-forms for $\alpha(z)$ and $\beta(z)$ are provided from $A(z)$ in classical analysis, for many leaky-wave antennas, $\alpha(z)$ and $\beta(z)$ are inter-dependent. Thus, one may not be able to choose a structure that yields the desired $A(z)$ distribution. Because of this, LWA designers often requires leaky-wave structures with independent control of both $\alpha(z)$ and $\beta(z)$ [2], [3], [6], [13].

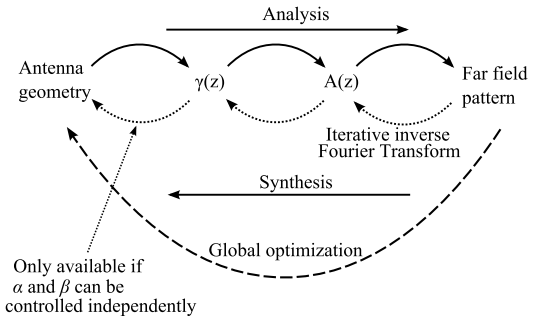

Fig. 8. Far-field pattern synthesis diagram of a leaky-wave antenna

In order to circumvent the above issues, a strategy based on a global optimization method, e.g. Genetic Algorithm (GA), can be used (Fig. 8, dashed line). To implement this strategy, the LWA is divided into a number of sections whose geometry can be set to vary linearly. The parameters for each section will be the optimization variables. The global optimization will utilize the proposed analysis for an accurate prediction of the near-field source distribution to compute the far-field pattern. With an appropriate cost function, the optimization will yield a close-to-best result that is available within the structure constraint. In fact, this method of using global optimization for LWAs was used by Siragusa *et. al.* in [37]. However, the process was based on full-wave numerical simulation of the LWA, which was very time-consuming, i.e. 2 weeks. Using the analysis proposed in this paper, a pattern synthesis problem may be carried out in less than 5 minutes on a typical desktop computer (provided the propagation constant γ is available for different structure cross-sections, as analytically, numerically or experimentally determined). It is emphasized that the final optimized result should be validated using full-wave simulation, in which one single simulation is typically sufficient.

It is noted that for most applications, we are not interested in the exact distribution of $E(\theta)$ for all angles but rather some characteristics of $E(\theta)$ need to be satisfied, such as low sidelobe level or maximum gain in a given direction. Thus, a cost function in the global optimization appears to be a very convenient tool to characterize performance.

The next section will demonstrate the results for two typical pattern synthesis requirements, namely targeting a low sidelobe level or a wide angular null in the far-field pattern. The structure under investigation will be, without restriction to the generality of the method, the HMSIW leaky-wave antenna. It is noted that, for a HMSIW with varying width, the attenuation constant α and phase constant β are inter-dependent and thus, the classical analysis can not be applied in these study cases.

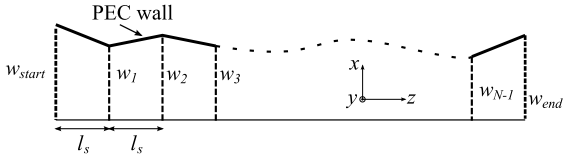

Fig. 9. The tapered HMSIW to be used for far-field pattern optimization (adapted from [14]).

V. Application: Specific Designs

In this section, the HMSIW is used as basis structure for designing LWAs targeting different far-field specifications. Only the width of the HMSIW is varied along the LWA $w = w(z)$. Other structures can be analyzed similarly with the (generally satisfied) prerequisites that the propagation constant $\gamma(z)$ can be found for a varying cross-section of the waveguide. A preliminary determination of γ can be carried out only once by analysis or simulation (as discussed in Section II) and stored in a library to be used in pattern synthesis process. In our investigation case, the analytical solution for the HMSIW found using the transverse resonance method [28] is used. The same substrate material as in Section III-B is selected. Two antennas have been designed and validated through experiment. Both antennas are terminated by a matched load. Design process and results are shown as follows.

A. Low Sidelobe Level

The HMSIW is divided into N sections in which the width of HMSIW is set to vary linearly as shown in Fig. 9. Each section has the same length of $l_s = L/N$. The desired far-field pattern has a maximum gain at angle θ_{tg} and lowest possible sidelobe level at the operating frequency f_0. Thus, the cost function can be chosen as

$$C_{LSL} = -c_1 G(f_0, \theta_{tg}) + c_2 SLL(f_0) + c_3 [G(f_0, \theta_{tg}) < G^*]. \quad (25)$$

The aim of the optimization is to reduce the cost function; hence, the weighting coefficients c_1, c_2, c_3 are positive to obtain a higher gain and lower sidelobe level (first and second terms in (25)). $G(f_0, \theta_{tg})$ is the realized gain at frequency f_0 and angle θ_{tg}, $SLL(f_0)$ is the sidelobe level at frequency f_0 considering the whole angular range. All terms are expressed in dB. The last term is equal to zero when $G(f_0, \theta_{tg}) \geq G^*$ and c_3 otherwise. This term is necessary to ensure that the optimization does not converge to a broadside LWA with extremly low sidelobe level but small gain at θ_{tg}. A value of 5 dB for G^* is sufficient to avoid the occurrence of this case. It is noted that since the third term provides a threshold G^* for the gain, it can alternatively be absorbed into the first term.

An optimization result is selected to demonstrate the method. The target frequency is $f_0 = 8$ GHz, the antenna length is $L = 8\lambda_0$ where λ_0 is the free-space wavelength at f_0, and the target direction of maximum radiation is $\theta_{tg} = 30°$. The number of section used in the optimization is $N = 50$ resulting in 50 variables in the GA. The number of approximately UTL in the analysis of each non-uniform HMSIW is 600 ($\Delta z = 0.5$ mm $= \lambda_0/75$). In this example, it is found that a value of $\Delta z \leq \lambda_0/20$ gives accurate enough results. Weighting coefficients in equation (25) are chosen such that c_1 and c_2 are in the same order, i.e. $c_1 = c_2 = 1$, while c_3 must be much larger than c_1 and c_2 to enforce the gain threshold, i.e. here $c_3 = 50$. A GA MATLAB code based on [38] has been implemented using one-point crossover method with a rate of 50% and uniform mutation with a rate of 2%. The population size is 80 genes and 8 bits are used to represent one variable, which results in 400 bits per gene. The typical number of generations required for convergence is about 50. It is noted that due to the efficient computation using the proposed method, a large population size can be used and a large number of generations can be computed, e.g. compared to [37]. Multiple optimization runs can be performed to validate and refine the optimized results.

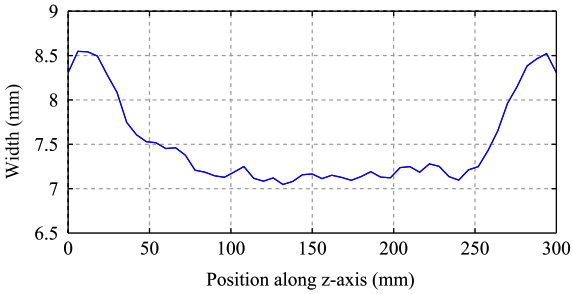

Fig. 10. Non-uniform HMSIW LWA shape optimized for low sidelobe level.

Fig. 11. Photograph of the fabricated antennas optimized for low sidelobe level (top) and wide null (bottom).

The optimized antenna profile is shown in Fig. 10, which demonstrates a similar shape as to the antenna designed in [39] targeting same optimization objective, i.e. low sidelobe level. In [39], a cosine field distribution is chosen primarily before calculating the width $w(z)$ while the method in the present paper demonstrates higher flexibility and accuracy in the pattern synthesis. A photograph of the fabricated antenna is displayed in Fig. 11 (top). It is noted that the PEC walls of the HMSIWs are realized by via holes through an accurate width-correction formula provided in [30]. The antenna is fabricated by a commercial company (Lintek) for high-quality prototype.

It is noted that the analysis (using the propagation constant calculated from [28]) assumes that conductor and dielectric losses are negligible, which is reasonable in the considered frequency range. Nevertheless, these losses can be taken into account in the model by including them into the overall α. The simulation results below are shown for the practical case with dielectric substrate loss tangent $\tan\delta = 0.0011$ and copper conductivity $\sigma = 5.8 \times 10^6 S/m$.

The aperture field distribution is shown in Fig. 12. Excellent agreement between analysis and full-wave simulation

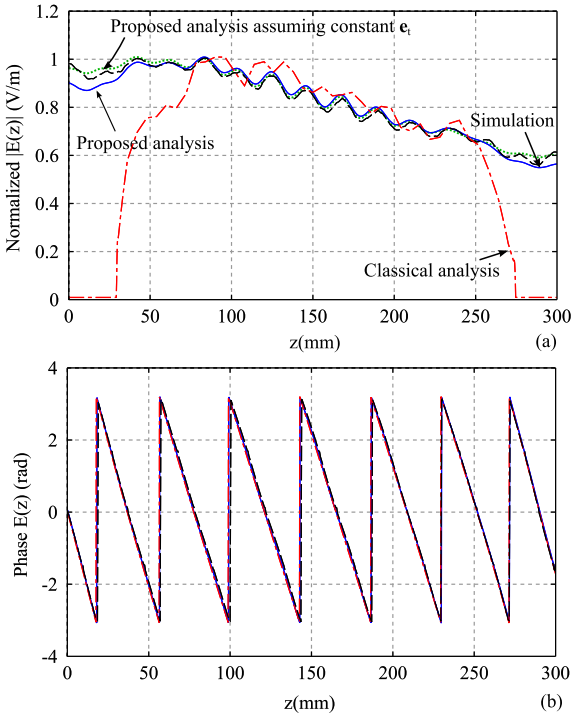

Fig. 12. Aperture field of the a non-uniform HMSIW optimized for low sidelobe level: (a) Magnitude; (b) Phase. The legends are the same for both figures and consistent with Fig. 4.

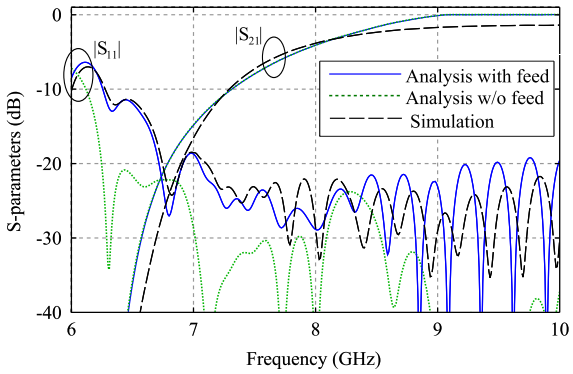

Fig. 13. Analyzed and simulated S-parameters for the HMSIW LWA optimized for low sidelobe level.

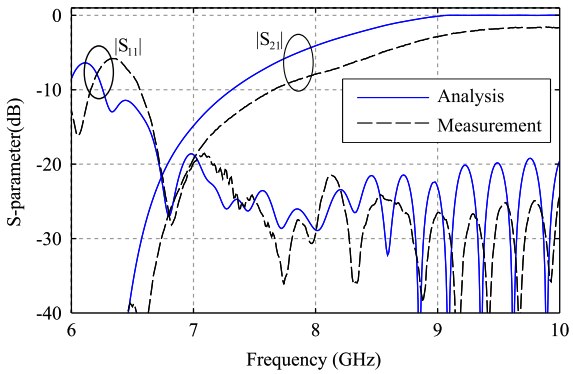

Fig. 14. Analyzed and measured S-parameters for the HMSIW LWA optimized for low sidelobe level.

is observed which further validates the proposed method demonstrated in section III-A. Since the width $w(z)$ does not vary significantly in this case, constant $\mathbf{e}_t$ can be assumed without losing much accuracy (green dotted curve in Fig. 12). This is an important point because in many cases, one can obtain a very good prediction of the near-field distribution without spectral modal analysis. In other words, only $\gamma(z)$ is required just as in the classical method.

The analytical and simulated results also indicate small distributed reflections along the antenna, which is expected for any non-uniform transmission line. As discussed before in section III-B, the result from the classical analysis shows large discrepancies, mostly at the transitions between slow-wave regions and fast-wave regions. It is also noted that the fluctuation in field distribution in the classical analysis does not arise from reflections since these are not taken into account. Rather, they arise from the fact that $\alpha(z)$ is varying along the antenna (equation (2)).

The analyzed and simulated S-parameters are shown in Fig. 13 with excellent agreement. For frequency $f \in (7, 10)$ GHz, since the transition provides a very good impedance matching to the antenna, the inclusion of the feed in the analysis is not necessary for this range. However for $f \in (6, 7)$ GHz, the inclusion of the transition in analysis (Section III-D) provides a much better prediction on the S-parameters of the whole structure. This might be crucial for wideband LWA design [8]. The measured S-parameters are shown in Fig. 14. Good agreement is also observed. The discrepancy in $|S_{21}|$ comes from the conductor and dielectric losses along the antenna, and also small radiation losses at the connectors, which are not taken into account in the analysis. However, this should not significantly affect the gain as validated by measurement (shown below).

The normalized far-field patterns at $f_0 = 8$ GHz are shown in Fig. 15. It can be observed that the classical approach provides correct calculation of the main beam. This is as expected since the phase $\psi(z)$ calculated from (4) is quite accurate (Fig. 12b). In fact, the only assumption on this equation is that the reflection along the antenna is negligible and it is well-known from array theory that the phase is more critical than amplitude in constructing the main beam of the radiation pattern. The classical calculation fails to obtain the number and level of sidelobes as well as null positions in the pattern. This is again as expected since it neglects the impact from slow-wave region (Fig. 12a). Furthermore, since the classical analysis neglects the reflection along the antenna, the predicted far-field distribution for back-ward wave, i.e. $\theta > 90°$ is always smaller than the true level.

Using the proposed analysis, very good agreement is obtained both with simulations (Fig. 15) and measurements (Fig. 16). The method predicts very well the relative sidelobe levels and null positions. The discrepancies towards $\theta = 0°$ and $180°$ are due to finite ground plane realization. The slight shift in maximum radiation angle can be attributed to the slight modification on the phase constant of the practical HMSIW compared to an ideal HMSIW (Fig. 3). The maximum sidelobe level is -21.5 dB in analysis and -23.8 dB in measurement. The calculated gain is 15.3 dB while the measured gain

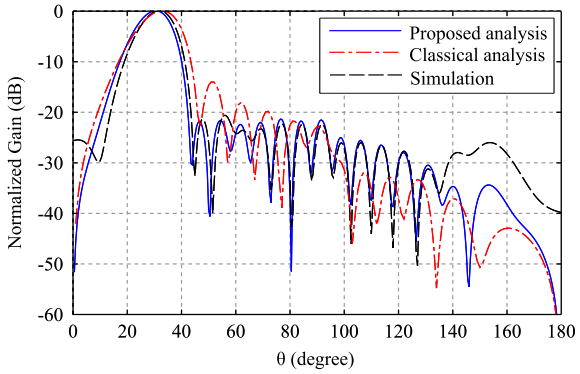

Fig. 15. Analyzed and simulated normalized radiation pattern at $f = 8$ GHz for the HMSIW LWA optimized for low sidelobe level.

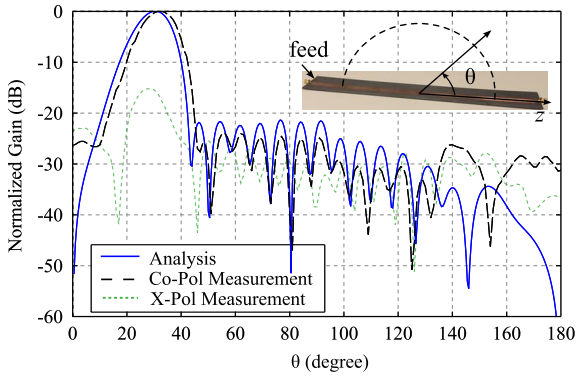

Fig. 16. Analyzed and measured normalized radiation pattern at $f = 8$ GHz for the HMSIW LWA optimized for low sidelobe level. The angle θ is defined as in the inset: $\theta = 90^\circ$ corresponds to broadside direction.

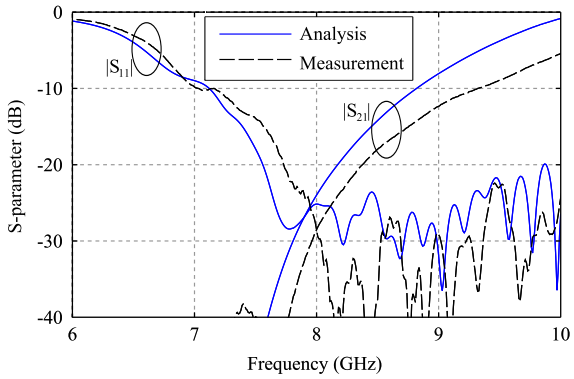

Fig. 17. Analyzed and measured S-parameters at $f = 8$ GHz for the HMSIW LWA optimized for wide null.

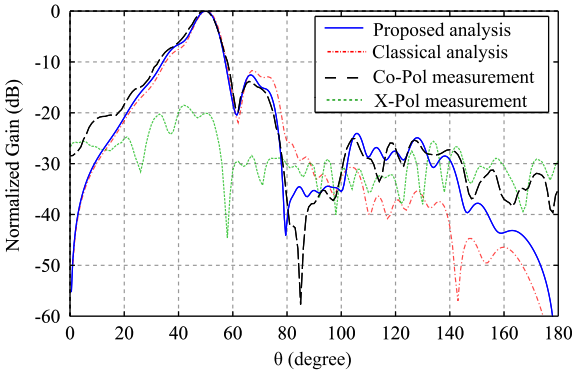

Fig. 18. Analyzed and measured normalized radiation pattern at $f = 8$ GHz for the HMSIW LWA optimized for wide null at $\theta_N \in (80^\circ, 100^\circ)$.

is 15.6 dB, which also shows a reasonable agreement. The measured cross-polarization level is less than -15 dB at the main beam.

B. Wide Null

In this section, a non-uniform HMSIW LWA with same material and thickness as previous section is optimized targeting a wide angular null around the broadside direction. The target of this illustrative optimization is to achieve an antenna with as high as possible gain at $\theta_{tg} = 50^\circ$, and as small as possible gain in the angular range $\theta_N \in (80^\circ, 100^\circ)$ given the structure material and thickness. The target frequency is $f_0 = 8$ GHz and the antenna length is chosen as $L = 10\lambda_0$, which is comparable with another design targeting similar specification [13]. The cost function can be modified from (25) as

$$C_{WN} = -c_1 G(f_0, \theta_{tg}) + c_2 Null(f_0, \theta_N) + c_3 [G(f_0, \theta_{tg}) < G^*] \quad (26)$$

where $Null(f_0, \theta_N)$ is the maximum gain in the range $\theta_N \in (80^\circ, 100^\circ)$ at the operating frequency f_0. For this optimization, the antenna is divided into $N = 30$ sections and the length of each approximately UTL is kept as $\Delta z = \lambda_0/75$. The same GA setup as for the previous case is utilized. The photograph of the fabricated optimized antenna is shown Fig. 11 (bottom).

Good agreement between the analyzed and simulated results for S-parameters can be observed in Fig. 17. It is noted that the feeding and termination transitions are included in the analysis. Similar features with the previous case are obtained if performing analysis without transition.

The analyzed and measured normalized radiation pattern are shown in Fig. 18. The measurement result demonstrates a LWA with a wide null at a level of -36 dB for $\theta \in (80^\circ, 98^\circ)$ and -32 dB for $\theta \in (80^\circ, 100^\circ)$. Again, very good agreement between analysis and measurement validates the accuracy of the proposed model as a significant improvement from the classical approach.

VI. Conclusion

A technique for accurate analysis and synthesis of non-uniform continuous-source LWA is introduced in this paper, which demonstrates higher accuracy on both near-field and far-field distributions of the antenna compared to the traditional approach. Using a circuit model, the method enables the inclusion of other circuit components, i.e. the feeding and termination transitions, with an improved accuracy on the whole system. Two LWAs based on HMSIWs have been optimized and demonstrated excellent measurement performances, which ultimately validate the proposed method. It is emphasized here that, under the assumption of single-mode propagation, this method is generally applicable for continuous-source LWAs with a reasonably smoothly varying structure. It may also be applied for periodic LWA with relatively small periodicity. In

this type of structures, the radiating elements are very close to each other, and thus can be approximated as a continuous-source structure.

APPENDIX A
ABCD - S PARAMETER CONVERSION

The conversion between S-parameters (**S**) and ABCD-parameters can be carried through the impedance matrix **Z**. As demonstrated in [7], for a traveling-wave

$$\mathbf{S} = \mathbf{U}(\mathbf{Z}-\mathbf{Z}_0)(\mathbf{Z}+\mathbf{Z}_0)^{-1}\mathbf{U}^{-1}, \quad (27)$$

$$\mathbf{Z} = (\mathbf{I}-\mathbf{U}^{-1}\mathbf{S}\mathbf{U})^{-1}(\mathbf{I}+\mathbf{U}^{-1}\mathbf{S}\mathbf{U})\mathbf{Z}_0. \quad (28)$$

where $\mathbf{Z}_0$ is a diagonal matrix whose elements are the characteristic port impedances $Z_0^{(i)}$ (the superscript $i = 1, 2$ denotes the port number), **U** is a diagonal matrix whose elements are the normalized constant of the traveling-wave defined in equation (9). With the normalization imposed in (10),

$$\mathbf{U} = \begin{bmatrix} \frac{\sqrt{Re(Z_0^{(1)})}}{|Z_0^{(1)}|} & 0 \\ 0 & \frac{\sqrt{Re(Z_0^{(2)})}}{|Z_0^{(2)}|} \end{bmatrix}. \quad (29)$$

The conversion between impedance matrix **Z** and ABCD-matrix **A** is well-known and can be derived easily from their definitions that relate the voltage and current between two ports,

$$\mathbf{Z} = \frac{1}{C}\begin{bmatrix} A & (AD-BC) \\ 1 & D \end{bmatrix}$$
$$\mathbf{A} = \frac{1}{Z_{21}}\begin{bmatrix} Z_{11} & (Z_{11}Z_{22}-Z_{12}Z_{21}) \\ 1 & Z_{22} \end{bmatrix}. \quad (30)$$

REFERENCES

[1] R. Honey, "A flush-mounted leaky-wave antenna with predictable patterns," *IRE Transactions on Antennas and Propagation*, vol. 7, no. 4, pp. 320–329, October 1959.

[2] C. Walter, *Traveling Wave Antennas*, ser. McGraw-Hill Electronic Science Series. McGraw-Hill, 1965.

[3] D. R. Jackson and A. A. Oliner, "Leaky-wave antennas," *Modern Antenna Handbook*, vol. 1, pp. 325–368, 2008.

[4] P. Burghignoli, F. Frezza, A. Galli, and G. Schettini, "Synthesis of broadbeam patterns through leaky-wave antennas with rectilinear geometry," *IEEE Antennas Wireless Propag. Lett.*, vol. 2, no. 1, pp. 136–139, 2003.

[5] J. Gómez-Tornero, A. Martínez, D. Rebenaque, M. Gugliemi, and A. Álvarez Melcón, "Design of tapered leaky-wave antennas in hybrid waveguide-planar technology for millimeter waveband applications," *IEEE Trans. Antennas Propag.*, vol. 53, no. 8, pp. 2563–2577, Aug 2005.

[6] J. Liu, D. Jackson, Y. Li, C. Zhang, and Y. Long, "Investigations of SIW leaky-wave antenna for endfire-radiation with narrow beam and sidelobe suppression," *IEEE Trans. Antennas Propag.*, vol. 62, no. 9, pp. 4489–4497, Sept 2014.

[7] R. B. Marks and D. F. Williams, "A general waveguide circuit theory," *Journal of Research - National Institute of Standards and Technology*, vol. 97, pp. 533–533, 1992.

[8] N. Nguyen-Trong, T. Kaufmann, and C. Fumeaux, "A semi-analytical solution of a tapered half-mode substrate-integrated waveguide with application to rapid antenna optimization," *IEEE Transactions on Antennas and Propagation*, vol. 62, no. 6, pp. 3189–3200, June 2014.

[9] K. Kurokawa, "Power waves and the scattering matrix," *IEEE Transactions on Microwave Theory and Techniques*, vol. 13, no. 2, pp. 194–202, Mar 1965.

[10] D. Frickey, "Conversions between S, Z, Y, H, ABCD, and T parameters which are valid for complex source and load impedances," *IEEE Transactions on Microwave Theory and Techniques*, vol. 42, no. 2, pp. 205–211, Feb 1994.

[11] R. Marks, D. Williams, and D. Frickey, "Comments on "conversions between S, Z, Y, h, ABCD, and T parameters which are valid for complex source and load impedances" [with reply]," *IEEE Transactions on Microwave Theory and Techniques*, vol. 43, no. 4, pp. 914–915, April 1995.

[12] D. Williams, "Traveling waves and power waves: Building a solid foundation for microwave circuit theory," *IEEE Microwave Magazine*, vol. 14, no. 7, pp. 38–45, Nov 2013.

[13] J. Gómez-Tornero, A. Martínez-Ros, and R. Verdú-Monedero, "FFT synthesis of radiation patterns with wide nulls using tapered leaky-wave antennas," *IEEE Antennas Wireless Propag. Lett.*, vol. 9, pp. 518–521, 2010.

[14] N. Nguyen-Trong, T. Kaufmann, L. Hall, and C. Fumeaux, "Optimization of leaky-wave antenna based on non-uniform HMSIW," in *IEEE MTT-S International Conference on Numerical Electromagnetic and Multipysics Modeling and Optimization*, August 2015, to be published.

[15] J. Liu, D. Jackson, and Y. Long, "Modal analysis of dielectric-filled rectangular waveguide with transverse slots," *IEEE Transactions on Antennas and Propagation*, vol. 59, no. 9, pp. 3194–3203, Sept 2011.

[16] ——, "Substrate integrated waveguide (SIW) leaky-wave antenna with transverse slots," *IEEE Transactions on Antennas and Propagation*, vol. 60, no. 1, pp. 20–29, Jan 2012.

[17] R. B. Marks, "A multiline method of network analyzer calibration," *IEEE Trans. Microw. Theory Tech.*, vol. 39, no. 7, pp. 1205–1215, 1991.

[18] Q. Lai, C. Fumeaux, W. Hong, and R. Vahldieck, "Characterization of the propagation properties of the half-mode substrate integrated waveguide," *IEEE Trans. Microw. Theory Tech.*, vol. 57, no. 8, pp. 1996 –2004, Aug. 2009.

[19] Q. Lai, C. Fumeaux, and W. Hong, "Periodic leaky-wave antennas fed by a modified half-mode substrate integrated waveguide," *IET Microw. Antennas Propag.*, vol. 6, no. 5, pp. 594 –601, 2012.

[20] G. Zelinski, G. Thiele, M. Hastriter, M. Havrilla, and A. Terzuoli, "Half width leaky wave antennas," *IET Microwaves, Antennas Propagation*, vol. 1, no. 2, pp. 341–348, April 2007.

[21] N. Nguyen-Trong, T. Kaufmann, and C. Fumeaux, "A wideband omnidirectional horizontally polarized traveling-wave antenna based on half-mode substrate integrated waveguide," *IEEE Antennas Wireless Propag. Lett.*, vol. 12, pp. 682–685, 2013.

[22] J. Xu, W. Hong, H. Tang, Z. Kuai, and K. Wu, "Half-mode substrate integrated waveguide (HMSIW) leaky-wave antenna for millimeter-wave applications," *IEEE Antennas and Wireless Propagation Letters*, vol. 7, pp. 85 –88, 2008.

[23] A. Martínez-Ros, J. Gómez-Tornero, F. Clemente-Fernández, and J. Monzó-Cabrera, "Microwave near-field focusing properties of width-tapered microstrip leaky-wave antenna," *IEEE Transactions on Antennas and Propagation*, vol. 61, no. 6, pp. 2981–2990, 2013.

[24] T. Tomofuji, H. Terada, S. Kawabata, K. Wakino, and T. Kitazawa, "Full-wave analysis and design of circular half-width microstrip leaky-wave antennas," *IEEE Transactions on Antennas and Propagation*, vol. 61, no. 8, pp. 3967–3975, 2013.

[25] D. Karmokar, D. Thalakotuna, K. Esselle, L. Matekovits, and M. Heimlich, "Reconfigurable half-width microstrip leaky-wave antenna for fixed-frequency beam scanning," in *2013 7th European Conference on Antennas and Propagation (EuCAP)*, 2013, pp. 1314–1317.

[26] D. Karmokar, D. Thalakotuna, K. Esselle, M. Heimlich, and L. Matekovits, "Fixed-frequency beam steering from a stub-loaded microstrip leaky-wave antenna," in *Proceedings of 2013 URSI International Symposium on Electromagnetic Theory (EMTS)*, May 2013, pp. 436–439.

[27] R. Henry and M. Okoniewski, "A broadside-scanning half-mode substrate integrated waveguide periodic leaky-wave antenna," *Antennas and Wireless Propagation Letters, IEEE*, vol. 13, pp. 1429–1432, 2014.

[28] E. F. Kuester, R. Johnk, and D. Chang, "The thin-substrate approximation for reflection from the end of a slab-loaded parallel-plate waveguide with application to microstrip patch antennas," *IEEE Trans. Antennas Propag.*, vol. 30, no. 5, pp. 910–917, 1982.

[29] J. Liu, D. Jackson, and Y. Long, "Propagation wavenumbers for half- and full-width microstrip lines in the EH_1 mode," *IEEE Transactions on Microwave Theory and Techniques*, vol. 59, no. 12, pp. 3005–3012, Dec 2011.

[30] F. Xu and K. Wu, "Guided-wave and leakage characteristics of substrate integrated waveguide," *IEEE Trans. Microw. Theory Techn.*, vol. 53, no. 1, pp. 66 – 73, Jan. 2005.

[31] N. Nguyen-Trong, T. Kaufmann, and C. Fumeaux, "Near-field characteristic of a wideband traveling-wave antenna based on a tapered half-mode substrate-integrated waveguide," in *2014 International Workshop on Antenna Technology (iWAT)*, Mar 2014, pp. 322–325.

[32] Y. J. Cheng, W. Hong, K. Wu, and Y. Fan, "Millimeter-wave substrate integrated waveguide long slot leaky-wave antennas and two-dimensional multibeam applications," *IEEE Transactions on Antennas and Propagation*, vol. 59, no. 1, pp. 40–47, Jan 2011.
[33] J. Hines, V. Rumsey, and C. Walter, "Traveling-wave slot antennas," *Proceedings of the IRE*, vol. 41, no. 11, pp. 1624–1631, Nov 1953.
[34] S. Podilchak, L. Matekovits, A. Freundorfer, Y. Antar, and M. Orefice, "Controlled leaky-wave radiation from a planar configuration of width-modulated microstrip lines," *IEEE Transactions on Antennas and Propagation*, vol. 61, no. 10, pp. 4957–4972, Oct 2013.
[35] A. Martinez-Ros, J. Gomez-Tornero, V. Losada, F. Mesa, and F. Medina, "Non-uniform sinusoidally modulated half-mode leaky-wave lines for near-field focusing pattern synthesis," *IEEE Transactions on Antennas and Propagation*, vol. 63, no. 3, pp. 1022–1031, March 2015.
[36] C. Caloz and T. Itoh, "Array factor approach of leaky-wave antennas and application to 1-d/2-d composite right/left-handed (crlh) structures," *IEEE Microwave and Wireless Components Letters*, vol. 14, no. 6, pp. 274–276, June 2004.
[37] R. Siragusa, E. Perret, P. Lemaitre-Auger, H. Van Nguyen, S. Tedjini, and C. Caloz, "A tapered CRLH interdigital/stub leaky-wave antenna with minimized sidelobe levels," *IEEE Antennas Wireless Propag. Lett.*, vol. 11, pp. 1214–1217, 2012.
[38] R. L. Haupt, "An introduction to genetic algorithms for electromagnetics," *IEEE Antennas and Propagation Magazine*, vol. 37, no. 2, pp. 7–15, Apr 1995.
[39] J. Guo, Z. Li, J. Wang, M. Chen, and Z. Zhang, "Analysis and design of leaky-wave antenna with low SLL based on half-mode SIW structure," *International Journal of Antennas and Propagation*, vol. 2015, Ariticle ID 570693, 5 pages, 2015.

Nghia Nguyen-Trong (S'12) dreceived the Bachelor's degree (first class Hons.) in electrical and electronic engineering from the University of Adelaide, Adelaide, S.A., Australia, in 2013. He is currently working toward the Ph.D. degree at the Adelaide Applied Electromagnetic Group, University of Adelaide.

His research interests include applications based on substrate-integrated waveguide technology.

Mr. Nguyen-Trong is one of the recipients for the undergraduate scholarship from the IEEE MTT-S in 2012. Based on his academic achievement, he received the Governor's International Student of Year of South Australia Award in 2012 and University Medal in 2014. He was one of the recipients of the Best Student Paper Award at the 2014 International workshop on Antenna Technology (iWAT). He also received the First Prize in the Student Paper Competition at the 2015 IEEE MTT-S NEMO Conference.

Leonard Hall (M'06) received his Bachelor of Electrical and Electronic and Ph.D. in Radio Frequency Engineering from the University of Adelaide, Australia, in 2000 and 2010 respectively. From 2005 to 2008 he was a Research Associate, responsible for GLIMMR 60 GHz 802.11 transceiver project, in the Electrical and Electronic Department of Adelaide University. He founded Freespace Solutions and worked as a consultant for DSTO and defence contractors as a subject matter expert in the area of radar, phased antenna arrays and transceiver systems from 2001 to 2009. In 2009 he joined the Australian Defence, Science and Technology Organisation as the Senior mm-Wave Technology Researcher in Radio Frequency Technologies group in Cyber and Electronic Warfare Division. Since 2014 he has also been an Associate Lecturer at the University of Adelaide.

Christophe Fumeaux (M'03–SM'09) received the Diploma and Ph.D. degrees in physics from the ETH Zurich, Switzerland, in 1992 and 1997, respectively. From 1998 to 2000, he was a Postdoctoral Researcher with the School of Optics, University of Central Florida, Orlando. In 2000, he joined the Swiss Federal Office of Metrology, Bern, Switzerland, as a Scientific Staff Member. From 2001 to 2008, he was a Research Associate and Group Leader with the Laboratory for Electromagnetic Fields and Microwave Electronics, at ETH Zurich, Switzerland. Since 2008, he has been with The University of Adelaide, where he is currently a Professor with the School of Electrical and Electronic Engineering. Since 2011, he is a Future Fellow of the Australian Research Council. His current main research interests concern computational electromagnetics, antenna engineering, THz technology and the application of RF design principles to optical micro/nano-structures.

Prof. Fumeaux has served as an Associate Editor for the IEEE Transactions on Microwave Theory and Techniques from 2010 to 2013. He serves currently as Senior Associate Editor for the IEEE Transactions on Antennas and Propagation. He was the recipient of the ETH Silver Medal of Excellence for his doctoral dissertation. He was the recipient/corecipient of best journal paper awards, including the 2004 ACES Journal and 2014 IEEE Sensors Journal, as well as best conference paper awards at the 2012 Asia-Pacific International Symposium on Electromagnetic Compatibility (APEMC 2012) and the 17th Colloque International sur la Compatibilité Electromagnétique (CEM 2014).